SAND2016-12415C

Spacecraft Pyroshock Attenuation in Three Parts

Vít Babuška[1] Steven Gomez[2] Scott Smith[3] and Christopher Hammetter[4]
Sandia National Laboratories, Albuquerque NM, 87106 USA

and

Dylan Murphy[5]
University of Georgia, Athens, GA, 30602, USA

Satellites are subject to pyroshock events that come from the actuation of separation and can be damaging events for satellites. The damage risk is mitigated by the fact that shock intensity is attenuated by the spacecraft structure. NASA and MIL handbooks and standards, which were developed from extensive tests performed in the 1960's, provide guidelines for estimating the attenuating effects of distance, joints, and other structural features in the load path between the shock source and the shock sensitive component. Anecdotal evidence suggests that these rules are not always conservative while sometimes they are grossly over-conservative. The first part of the paper summarizes and interprets the attenuation rules-of-thumb. The second part presents a case study in which attenuation factors developed for a satellite are compared to attenuation factors measured in a pyro-shock test of the satellite. The third part looks at the feasibility of using 21st century computational tools to predict shock attenuation through a simple jointed structure. Such tools have the potential to recreate satellite specific shock attenuation factors that could provide greater confidence in the predicted loads on shock sensitive components by reducing, and perhaps eliminating, the over-under conservatism issue; however they are surprisingly difficult to use.

I. Introduction

SATELLITES are subject to pyroshock events during the launch phase that come from the actuation of separation devices. The shocks are very short, high intensity events with high frequency content that can be damaging events for satellites. Near the source, peak accelerations are on the order of a thousand G's. The damage risk is mitigated somewhat by the fact that the shock intensity is attenuated by the spacecraft structure. The attenuation of pyroshocks is addressed in NASA and MIL handbooks and standards. These documents provide guidelines for estimating the attenuating effects of distance, joints, and other structural features in the load path between the shock source and the shock sensitive component. Anecdotal evidence suggests that these rules are not always conservative while sometimes they are grossly over-conservative. Neither situation is good. In the first case, overestimating the attenuation can lead to increased risk of a pyroshock induced failure; in the second case, it can lead to unnecessary and expensive overdesign for a phantom risk.

The guidelines in the NASA and MIL standards[1-4] were developed from extensive tests[5,6,7] performed in the 1960's. This was a long time ago and the origins of the guidelines have largely been forgotten or never passed on to current spacecraft engineers. The materials used in satellites today are different than those used in the 1960's. A better understanding of the bases for the information in the NASA and MIL standards could improve systems engineering and spacecraft designs.

---

[1] Principal Member of the Technical Staff, Environments Engineering and Integration Dept., Mail Stop 0557, Associate Fellow AIAA
[2] Member of the Technical Staff, Component Science & Mechanics Dept., Mail Stop 0346
[3] Graduate Intern, Structural Dynamics Dept., Mail Stop 0557
[4] Senior Member of the Technical Staff, Solid Mechanics Dept., Mail Stop 0840
[5] Student, Mechanical Engineering Dept., 597 D. W. Brooks Dr. Athens, GA 30602

Computational analysis software is more sophisticated and capable than ever today. These simulation tools have the potential to create satellite specific shock attenuation factors, which could provide greater confidence in the predicted loads on shock sensitive components by reducing, and perhaps eliminating, the over-under conservatism issue that comes from using general guidelines. In fact, NASA-HDBK-7005 anticipated this evolution in 2001:

> "However, with the rapidly increasing capabilities of computer hardware and software, it is possible that finite element method (FEM) models may be developed in the future that can successfully predict these local inputs with sufficient accuracy for design applications." – NASA HDBK-7005 Section 8.3 High Frequency Transient Responses, page 197, 2001.

The objectives of this paper are three. First, the NASA standards that address pyroshock for satellite systems are summarized (MIL standards[8,9,10] are largely the same) and the original studies are discussed. Pyroshocks on launch vehicles (e.g., stage separation with mild detonating fuses (MDF)) are not discussed. Next, a case study is presented in which attenuation factors developed for a satellite are compared to attenuation factors measured in a pyro-shock test of the satellite. The attenuation factors were based on the NASA standards but tailored to the satellite specific load path. The last section presents results from a numerical study of pyroshock through a simple jointed structure using high-performance computing tools. The computational simulations are compared to laboratory tap tests highlighting some of the promises and pitfalls of using 21st century computational tools to predict joint specific shock attenuation.

II. Pyroshock Attenuation Guidelines

Pyroshock is one of the environments in which satellites and their subsystems and components must be tested during environmental testing. A pyroshock test simulates the transient loads created when explosive devices, (e.g., squibs) release launch locks and clamping mechanisms for deployment of antennas, solar arrays, etc. Pyroshock events are short duration (< 20 msec) high amplitude, high frequency transient excitations. However, long before a satellite reaches the environmental testing phase, decisions must be made regarding loads on potentially shock sensitive components so they can be designed. This requires an understanding not only of the pyroshock excitation, but also of the loads the shock produces on the components of interest. The pyroshock loads experienced by a component are very dependent on the proximity of the component to the source of the shock. Because of short duration and high frequency nature of a pyroshock, it will be attenuated by the structural features in the load path between the pyroshock source and the component. The attenuation effects have been handled empirically with guidelines or rules in NASA handbooks[1-4]. Almost all the recommended attenuation factors in the NASA handbooks come from a study performed by the Space System Dynamics Unit of Martin Marietta Corporation for Goddard Space Flight Center between 1968 and 1970[5,6]. The objective of that effort was to provide a single reference for shock data compiled from pyroshock data from the aerospace industry.

The pyroshock environment is usually divided into three regions[3]: near-field, mid-field, and far-field. The near field is roughly within 6 inches of the source and the shock effects are due to the propagation of stress waves[13]. The peak acceleration levels can be greater than 10 kG and spectral bandwidth can extend beyond 10 kHz. In the mid-field (shock path distance > 6 in) the responses to a shock are a combination of oscillatory response and wave propagation effects. A widely accepted rule-of-thumb is that the peak accelerations and spectral bandwidth are reduced by factors of 10 from near-field levels – i.e. peak acceleration < 1000G and spectral content between 3 kHz and 10 kHz. In the far-field, the structure has transformed the stress waves into oscillatory responses dominated by the structural resonances. Peak accelerations and spectral bandwidth are further attenuated.

Only the mid-field and far-field regions are of interest in this paper and generally in spacecraft design. This is why pyroshock specifications are written in terms of the max-max absolute acceleration (MMAA) Shock Response Spectrum (SRS), but extending up to 10 kHz - 50 kHz. A quality factor (Q) of 10, corresponding to a 5% damping ratio, is used exclusively. A pyroshock SRS is characterized by a ramp portion with a slope of ~30 - 40 dB per decade (9 – 12 dB/octave) and a flat portion above the knee frequency. The knee frequency is the 1st resonant frequency in the SRS. The SRS does not contain a duration, but it is understood that the duration of the pyroshock transient is on the order of 20 msec. Unlike other mechanical shock insults, pyroshocks do not introduce a velocity change. A typical maximum predicted environment (MPE) SRS specification is shown in Figure 5. Note that an SRS can be used to describe the near-field pyroshock to some extent but the knee frequency is greater than 10 kHz, making it not very practical.

Understanding the pyroshock event is necessary but insufficient. The pyroshock environment must be evaluated for shock sensitive parts. Because of the high-frequency character of a pyroshock, small parts, brittle parts and circuit board elements are most at risk[1]. However, it is not possible to define a pyroshock environment at specific

shock sensitive parts inside a component; they are simply too small. The pyroshock SRS are used primarily to establish test environments for components (i.e., electric boxes) mounted on the spacecraft structure. These environments are used to design tests to verify the component's robustness to pyroshock transients, or to exempt a component from shock testing requirements. For example, MIL-HDBK-340A[9] exempts units from shock qualification testing if:

1) The qualification random vibration test spectrum when converted to an equivalent shock response spectrum (3-sigma response for Q = 10) exceeds the qualification shock spectrum requirement at all frequencies below 2000 Hz.
2) The maximum expected shock spectrum above 2000 Hz does not exceed G values equal to 0.8 times the frequency in Hz at all frequencies above 2000 Hz, corresponding to a velocity of 1.27 meters/second (50 inches/second).

Both criteria must be satisfied, so understanding the attenuation of the pyroshock transient between the source and the component containing shock sensitive parts is important.

The attenuation of the pyroshock event is affected by shock magnitude, materials and material changes, shock load path distance, redundant shock load paths, changes in cross-sections, structural geometry discontinuities, and joints in the shock load path. Probably the dominant contributor to shock attenuation is the structure geometry, but this is design specific and therefore impossible to generalize. Only two structural attenuation features are specifically addressed in NASA and MIL documents: distance (which means shock path distance) and joints. Neither takes into account sensitivity to shock magnitude.

A. Attenuation with Distance

NASA-HBDK-7005 and NASA-STD-7003A provide guidance on shock attenuation as a function of shock path distance from the source. Perhaps the most widely quoted shock attenuation curve in NASA-HBDK-7005 is Figure 5.7, shown in Figure 1. This figure shows the amount of attenuation for the SRS ramp and the SRS plateau. The original source of this curve is Ref. 7, which described pyroshock test requirements for Viking lander capsule components. This attenuation model was derived from Refs. 5 and 6, specifically for the Viking lander capsule. No uncertainty data are provided nor is an explanation of how the curves were derived. Since these curves were included in NASA HDBK-7005, they have been used for all kinds of vehicles, presumably successfully, but the fact remains that they were derived for a specific vehicle so extrapolation to any other vehicle should be done with full knowledge of its origin.

Reference 5 presented an exponential model of peak acceleration attenuation for truss and cylindrical shell structures from 456 shock test measurements. The attenuation rates from the truss data are shown in Figure 2. The overall mean attenuation coefficient, α, is 0.033 and the associated coefficient of variation is 27%. The attenuation coefficients vary from 0.023 to 0.044. References 5 and 6 do not provide enough information to determine if there are joints in the shock path or the truss materials.

There are other attenuation models in NASA-HBDK-7005 that one can evaluate for their specific application. As a point of comparison, Eq. 5.78 in NASA-HBDK-7005 is evaluated at 2 kHz, a typical knee frequency in a pyroshock specification, and compared to the mean attenuation from the truss data in Ref. 5 (Figure 2), in Figure 3. The response at the knee frequency is usually the peak response in the SRS, so this is the best frequency at which to compare the SRS attenuation with peak acceleration attenuation. The difference is large, and it suggests that scaling rules should be based on data sources and structures similar to the spacecraft for which environments are being developed. Furthermore, it reinforces the point that environments and data in NASA handbooks and MIL standards should only be used when nothing better is available.

Note that shock test MMAA SRS amplitude tolerances are typically[3]:

a) +/- 6 dB at natural frequencies <= 3 kHz;
b) +9/-6 dB at natural frequencies > 3 kHz.

So if the attenuation is less than the test tolerance it is likely to be swamped by the

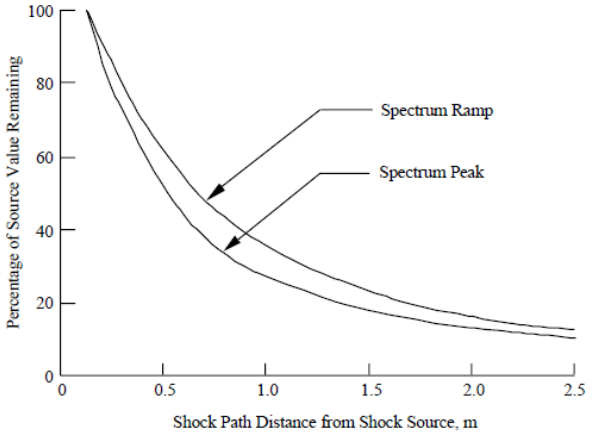

FIGURE 5.7. Shock Response Spectrum Versus Distance from Pyroshock Source.

Figure 1. SRS vs. Distance from Pyroshock Source Excerpt from NASA-HDBK-7005[1]

uncertainty in the shock test environment to which the component is exposed. Also, shock path distance may be difficult to establish so that uncertainty should be taken into account.

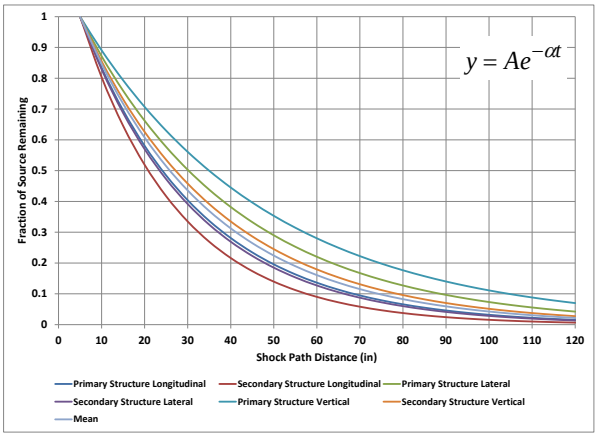

Figure 2. Attenuation Rates for a Truss Structure from Ref. 5

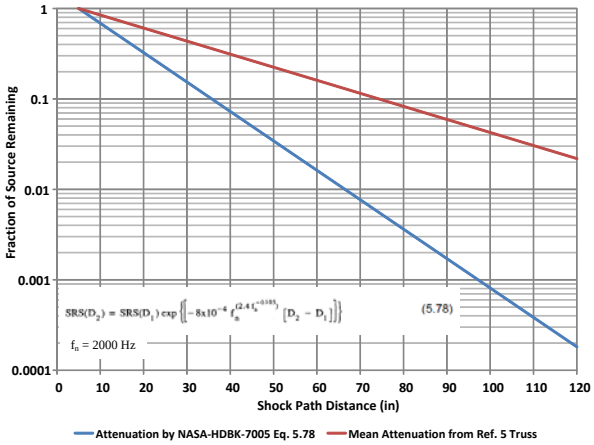

Figure 3. Comparison of Attenuation Models for Distance

B. Attenuation across Joints and Structural Discontinuities

NASA-HDBK-7005 provides guidance regarding the amount of attenuation across joints. The guidance comes from a paragraph in Ref. 7 that describes pyroshock test requirements for the Viking lander. It reads:

> "… to ensure adequate conservatism it was elected to use the following approach to joint attenuation: Assume a peak attenuation of 40% for each joint, up to a maximum of three joints, with no attenuation applied to the ramp of the spectrum."[7].

This is the so-called "3-joint rule" that is specified in various other documents, such as Refs. 4 and 12. This 3-joint rule essentially limits the amount of attenuation from joints in the shock path to 13 dB, regardless of the type of joints, the shock amplitude or the number of joints if there are more than three. The 3-joint rule is not unreasonable because some types of joints such as bolted joints lose their attenuating properties as excitation amplitudes decrease. The 3-joint rule would be better interpreted as a "3-joint guideline" and applied with additional, design specific information.

More nuanced information is provided in Ref. 6. In this reference, attenuation ranges are assigned to specific interface types. Solid joints and riveted butt joints provide no attenuation. A matched angle joint reduces the shock pulse by 30-60% and a solid joint with interface material provides a reduction of 0-30%. Load path bifurcations are discussed briefly also. The amplitude of a shock may be reduced by 20% to 70% when there is a corner in the shock path.

Shock attenuation effects across joints and structural features are complicated and not well understood. All information in the MIL and NASA handbooks is quite crude and should be used as a guideline rather than as a rule. Vehicle specific testing is still the best way to reduce uncertainty and avoid the risks associated with over- or under-conservatism.

III. Pyroshock Attenuation Case Study

This section describes a more nuanced approach to estimating and applying shock attenuation factors that simply following the guidelines in the NASA and Mil standards. Shock attenuation factors were estimated for a satellite payload during the preliminary design phase to provide loads on various components on the satellite. The payload underwent a simulated pyroshock test during its environmental testing. The test provided data that permits a direct assessment of the adequacy of the estimated shock attenuation factors that were assumed during preliminary design.

The satellite addressed herein is a secondary payload, attached to the spacecraft bus by seven struts in a tripod configuration. Shocks are transmitted from the bases of the struts throughout the payload. The load path and the amount of attenuation at shock sensitive components are shown in Figure 4. Shock attenuation factors for typical structural components are tabulated in Table 1. The attenuation levels were computed by aggregating the effects of structural features in the load path. These design factors should be conservative, but not excessively so.

There are two primary load paths from a shock applied at the base of a strut to subsystems and components. The attenuation across a strut was estimated as 13 dB based on the design of the strut. The largest attenuation factor was 30 dB at subsystem G, which is far down one of the load path

During the test, different shocks were specified for the front feet and the back foot. The shock response spectra specifications (SRS) are shown in Figure 5. This specification is typical of a pyroshock. There is little velocity change in a pyroshock so the SRS slope will be effectively zero at low frequency. This frequency range is not shown in Figure 5. In these tests the velocity change was on the order of 10 ft./sec. The slope of the SRS is approximately 2 in log-log space. The SRS high frequency asymptote is the amplitude of the shock[13]. The breakpoint natural frequency is 2 kHz suggesting that the resonant frequency content of the shock starts at that frequency.

The shocks were applied to the strut feet through a resonant beam (Figure 6) impacted by a projectile fired from a shock actuator air gun (Figure 7). The resonant beam was bolted to a foot pad and an accelerometer was mounted on the beam near the pad as shown in Figure 8. This accelerometer response was taken as the shock input. Figure 9 shows a typical time history measured with a pad accelerometer and its corresponding SRS. The acceleration depends on the speed of the projectile which was difficult to set with precision. This impact was above the specified level and somewhat out of tolerance.

In this paper, shock attenuation is defined as the ratio of the response SRS to the input SRS. Due to the complex load paths, and to avoid having to deal with different coordinate frames, the input and response SRS were each root sum squared (RSS'd) first. The frequency region of primary interest is 2 kHz to 10 kHz. Attenuation factors for three components: struts, component 18 and subsystem G in Figure 4 are presented.

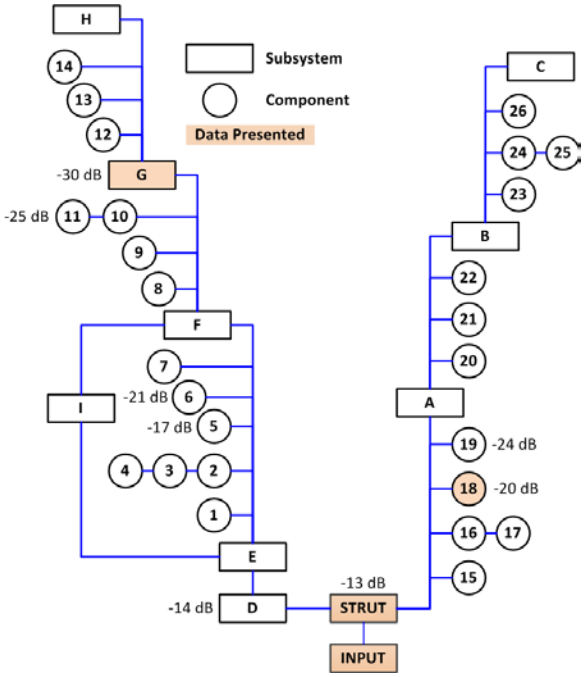

Figure 4. Load Path and Predicted Attenuation Factors

Table 1. Typical Structural Attenuation Factors

Structural Feature	Attenuation
Rotational Joint	3 dB
Distance	3 dB
Right Angle	0 dB
Bolted Joint	3 dB
Bonded Joint	1 dB
Flexure	0 dB
Material	1 dB

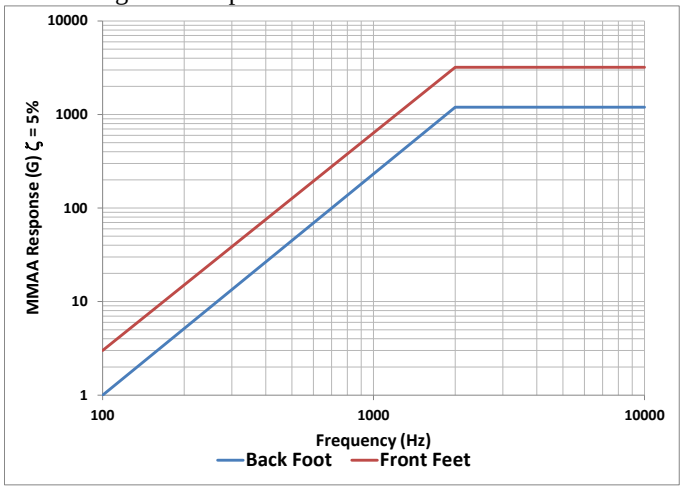

Figure 5. Input Shock Response Spectra Specifications

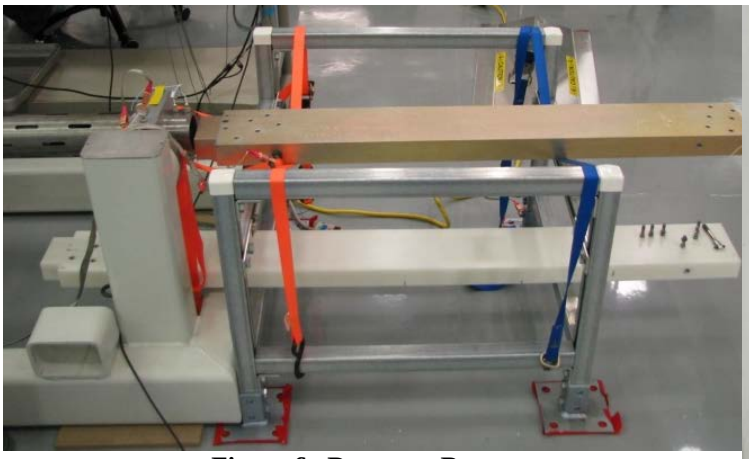

Figure 6. Resonant Beam

Figure 7. Shock Actuator

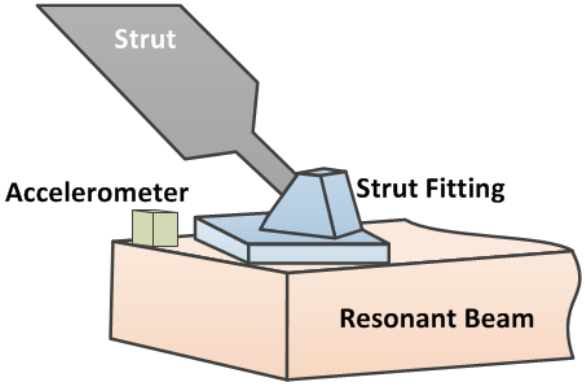

Figure 8. Resonant Beam Strut Interface

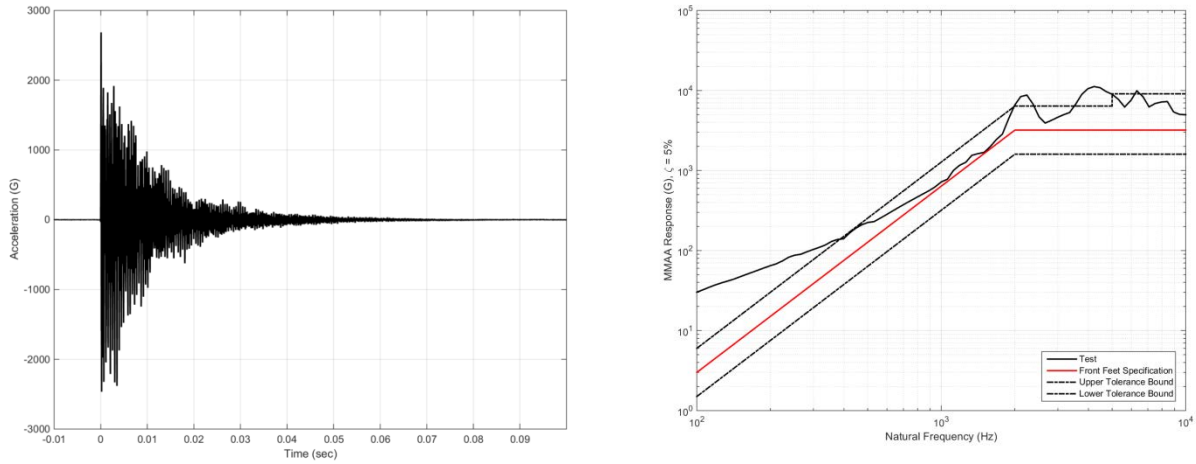

(a) Input Shock Acceleration (b) Input Shock SRS

Figure 9. Typical Input Shock at the Strut Fitting

C. Strut

Figure 10(a) shows the measured attenuation across a strut for an input applied to the left foot in the Y-axis. The system has multiple struts and there were five accelerometers attached near the ends of the struts. The mean attenuation (i.e., the average over the five sensor locations) of the shock applied at the base of the left struts is more than the predicted attenuation of 13dB. Figure 10(b) shows the attenuation across one of the right struts. The mean

attenuation also is greater than the predicted attenuation of 13dB. However, the attenuation measured at one sensor (Z4) was less than expected for both shocks. If there had been a shock sensitive part near Z4, then it could have been at risk. Ideally it would have been identified as a potential risk through modeling before the system was shock tested.

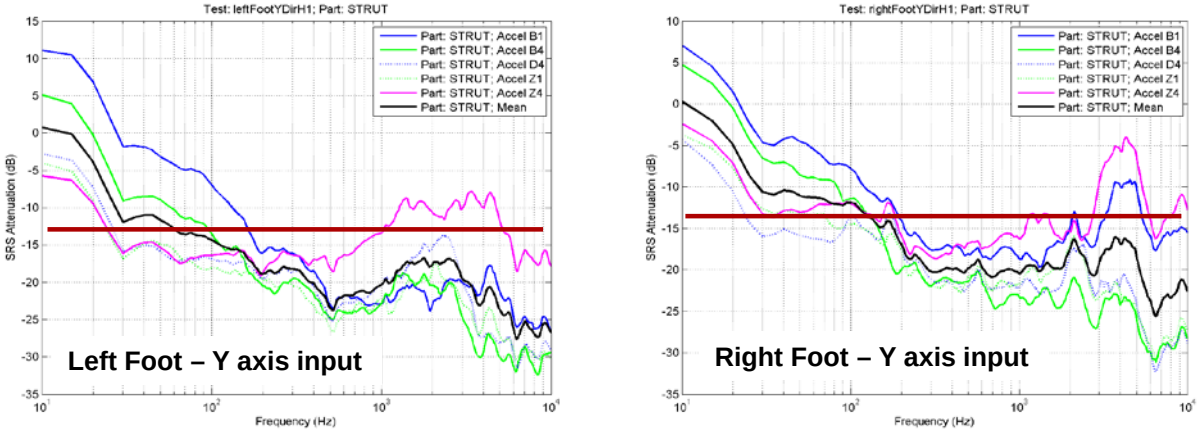

(a) Y-axis Attenuation; Input at Left Foot (b) Y-axis Attenuation; Input at Right Foot

Figure 10. Attenuation across a Strut

D. Component 18

The shock attenuation factor for Component 18 was estimated as 20 dB. Two accelerometers measured the response of the component. The 20 dB attenuation factor was conservative above 2 kHz as illustrated by the SRS attenuations shown in Figure 11. There is a resonance at 4500 Hz that is excited by the shock applied to the right foot. The magnitude of the shock had been sufficiently attenuated by the time it reached the component. However, the resonances around 400 Hz could have been problematic; happily they were not.

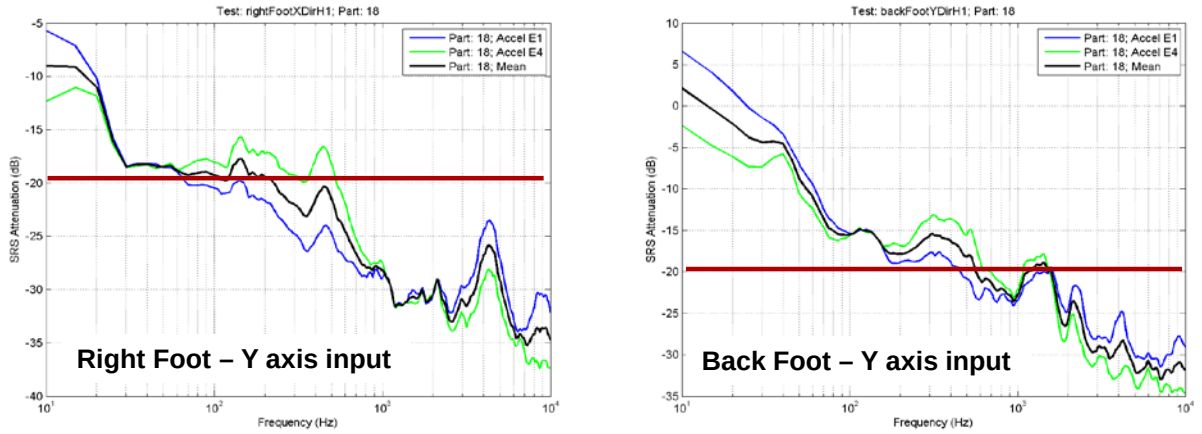

(a) Y-axis Attenuation; Input at Right Foot (b) Y-axis Attenuation; Input at Back Foot

Figure 11. Attenuation at Component 18

E. Subsystem G

Subsystem G is far away from the shock input locations and the shock has to traverse many structural features to get there as evidenced by the 30 dB attenuation factor. There were four accelerometers distributed on this subsystem for the shock test. Figure 12 shows the attenuation to shocks applied in the x-axis at the left and right feet. There is a clear resonant response around 2200 Hz that affects the amount of attenuation experienced locally at sensor O1. A resonant response is also observable at 400 Hz, which is well below the corner frequency of the environment. While the average attenuation is larger than the predicted attenuation factor, locally (at sensor O1) the shock attenuation is only 20 dB. This illustrates both the benefits and risks of using relatively coarse design factors.

The attenuation factor was conservative when compared to the mean of the measured locations above the knee frequency. Since the attenuation factors were developed early in the program they cannot be expected to be precise at specific locations on components that had not been designed or test accelerometer locations defined.

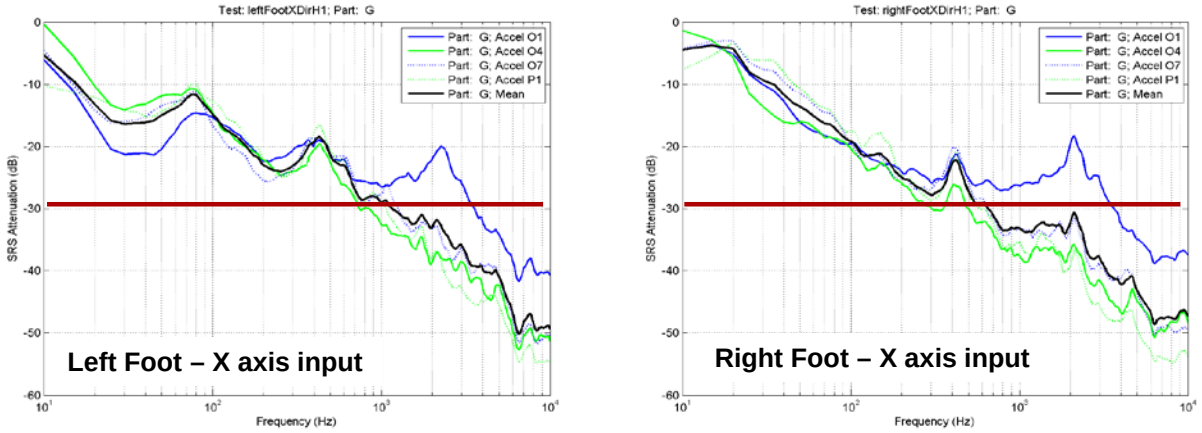

(a) X-axis Attenuation; Input at Left Foot (b) X-axis Attenuation; Input at Right Foot

Figure 12. Attenuation at Subsystem G

IV. Pyroshock Attenuation Modeling

Numerical analysis tools are much more capable today than they were in the 1960's when NASA was studying pyroshock and developing the empirical rules contained in the NASA handbooks and standards. Structural analysis tools such as ABAQUS and Sandia National Laboratories' Sierra Solid Mechanics Presto have the potential to enable engineers to relatively easily create satellite specific joint models from which to estimate shock attenuation factors. This could provide greater confidence in the predicted loads on shock sensitive components by reducing and perhaps eliminating the over-/under-conservatism issue. Kolaini[15] investigated the feasibility of using high-fidelity wave propagation finite element codes to predict displacements in a complex component from a shock input. One conclusion from the study was that it was a challenge both technically and computationally.

To assess the feasibility and level of difficulty of these tools for this application, a simple beam with a lap-joint was studied both computationally and experimentally. The beam is a benchmark nonlinear beam structure, commonly termed the Brake-Reuss Beam (BRB)[14]. The beam is a 28.25" long, 1 in^2, steel beam with a bolted lap joint and three 5/16"-24 bolts as shown in Figure 13.

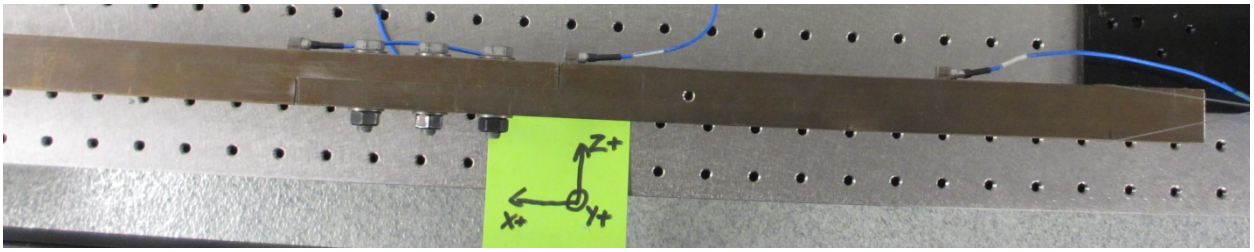

Figure 13. Sandia National Laboratories Brake-Reuss 3-Bolt Lap Joint Beam

A. Numerical Results

For the numerical experiments, the beam was modeled in Sierra Solid Mechanics Presto and explicit solutions for different loading cases were computed. Figure 14 shows the mesh used in the model. Prescribed axial (Z-axis) force or acceleration boundary conditions were applied to the nodeset at the left end of the beam. The output quantities were average cross sectional accelerations of nodesets at the left, left-mid, right-mid and right end. There are 99 nodes in the output nodesets, shown in yellow in Figure 14.

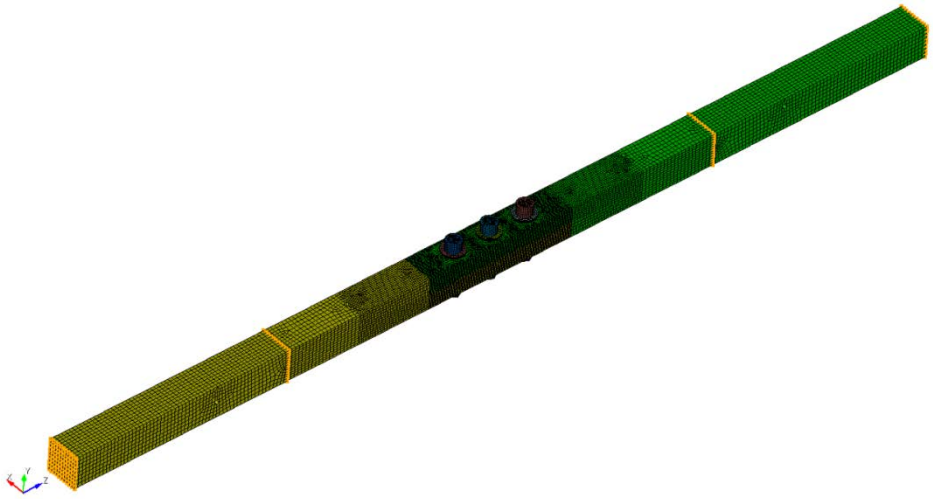

Figure 14. Sierra SolidMechanics Mesh of Brake-Reuss 3-bolt Lap Joint Beam

The bolts were preloaded prior to applying a load by creating three material block sections of each bolt: bolt shaft, bolt head/nut, and washers. The bolt shaft was contiguously meshed to the upper bolt head, lower beam nut, and washers (i.e., they shared the same nodes). These bolt shaft, head, nut, and washer assemblies were not contiguously meshed with the lap joint bars and were allowed to contact through a constant coulomb friction coefficient of 0.7 (Steel-Steel). The middle section of the bolt was artificially strained along the axis of the bolt, causing the bolt head, nut, and washer assembly to compress against the beam, simulating tightening. The bolt washer and beam contact surfaces were used to monitor the axial force which allows for calibration of the bolt preload. The bolt torque was related to the bolt tension (preload force) with

$$F_i = \frac{T}{Kd} \tag{1}$$

where K is the nut factor, d is the tensile stress diameter of the bolt, and T is the bolt torque. For the present study, $K = 0.2$ is used, which is standard for most bolts. The first 0.004 msec of simulation time were allocated to achieving a stable bolt preload force, followed by the respective pulse width of input force or acceleration. Simulation run times were on the order of 3 hours clock time for 20 msec of simulation. The time step used was 47.9 nanoseconds.

A near net zero velocity change 200 N impact (Figure 15) was applied to each node in the node set on the left side of the beam, giving the beam effectively a 20 kN hit. Two cases, distinguished by bolt torque, were simulated. Bolt torques of 11 ft-lb (14.9 N-m) and 27 ft-lb (36.6 N-m) were modeled. The bolt torques are typical for the bolt sizes. The average axial acceleration at the left-mid node set and the corresponding SRS for the 11 ft-lb bolt torque case are shown in Figure 16. The same data from the 27 ft-lb bolt torque case are shown in Figure 17. The differences in the responses are larger than expected. Some of the difference can be attributed to the clamping force difference but part of it may be numerical artifacts associated with the bolt preloading.

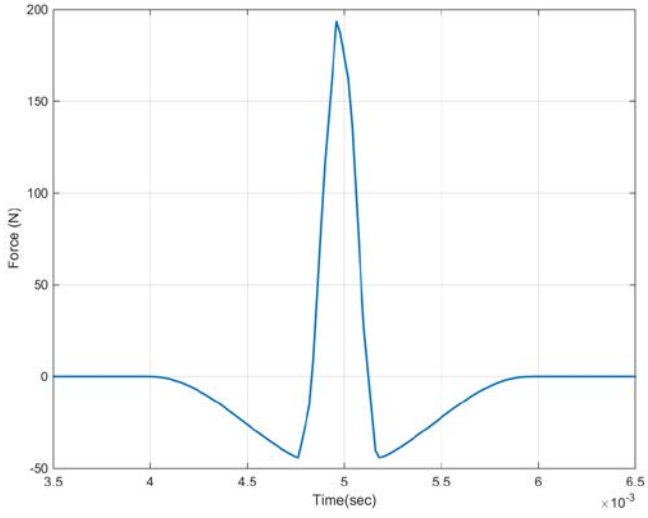

Figure 15. Applied Nodal Force at the Left End Node Set

The SRS attenuation across the lap-joint is shown in Figure 18 for each bolt preload case The SRS of the average axial accelerations at the left-mid and right-mid node sets are shown in Figure 19,. The simulations show no attenuation across the lap joint. The SRS are within typical shock test MMAA SRS

amplitude tolerances. In fact the SRS amplitude on the right side of the joint is higher above 4 kHz than the left side of the joint. This is counterintuitive and may be due to the specific axial location of the node sets and numerical artifacts. There should be more dissipation at lower bolt torques, but at the torques used, the Brake-Reuss beam essentially behaves as a solid, joint free bar.

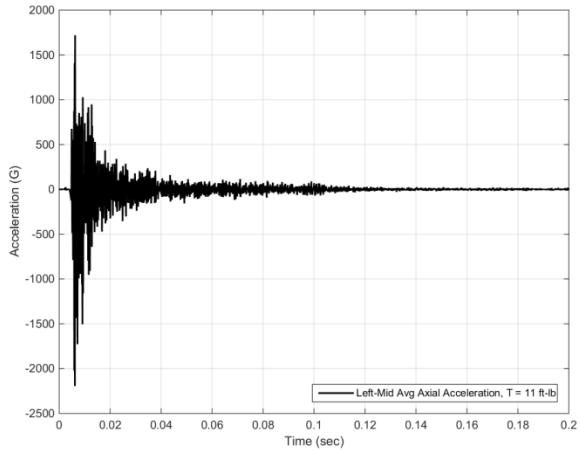

(a) Average Axial Acceleration of Left-Mid Node Set (T = 11 ft-lb)

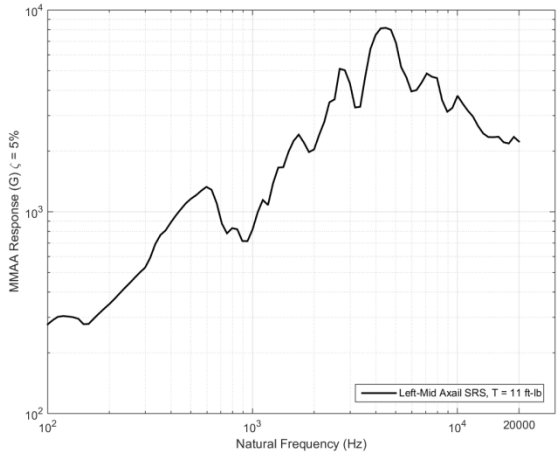

(b) SRS of Left-Mid Node Set Average Axial Acceleration (T = 11 ft-lb)

Figure 16. Axial Acceleration and SRS at Left-Mid Location (T = 11 ft-lb)

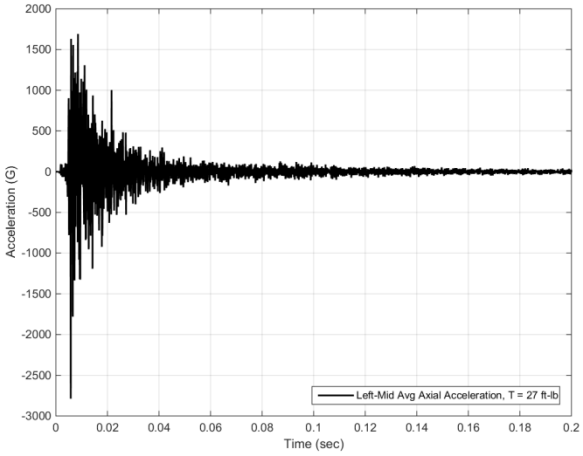

(a) Average Axial Acceleration of Left-Mid Node Set (T = 27 ft-lb)

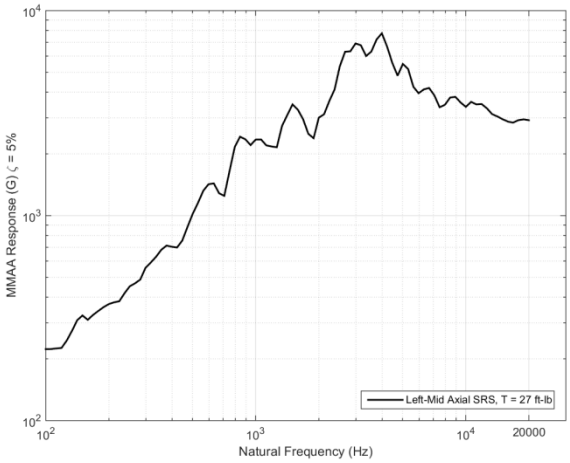

(b) SRS of Left-Mid Node Set Average Axial Acceleration (T = 27 ft-lb)

Figure 17. Axial Acceleration and SRS at Left-Mid Location (T = 27 ft-lb)

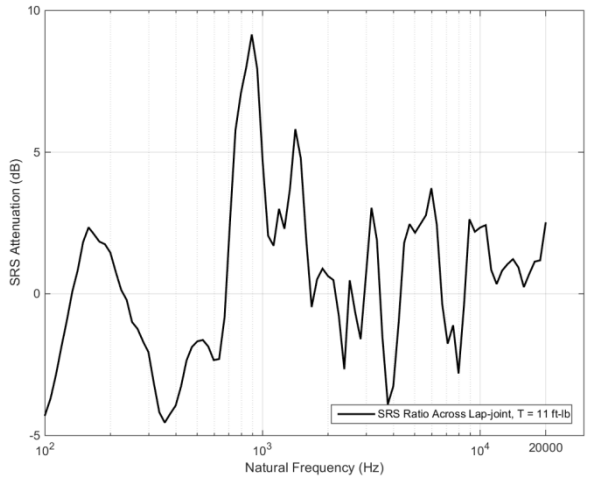

(a) SRS Lap joint Attenuation Factor (T = 11 ft-lb)

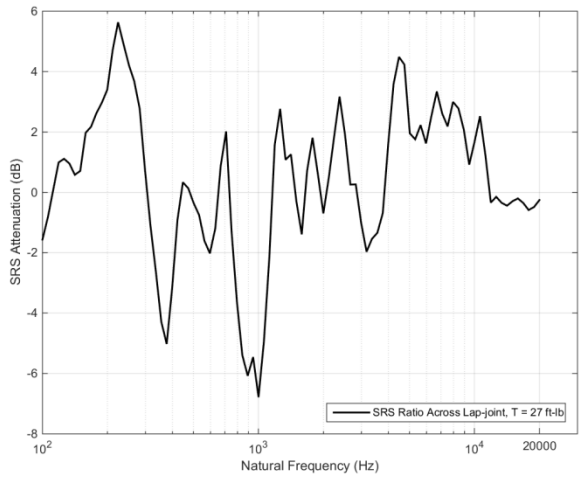

(b) SRS Lap joint Attenuation Factor (T = 27 ft-lb)

Figure 18. SRS Attenuation Across the Lap Joint

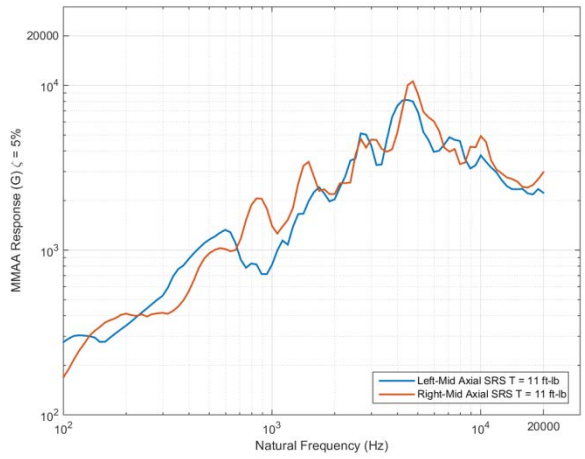

(a) SRS of Left-Mid and Right-Mid Node Set Average Axial Accelerations (T = 11 ft-lb)

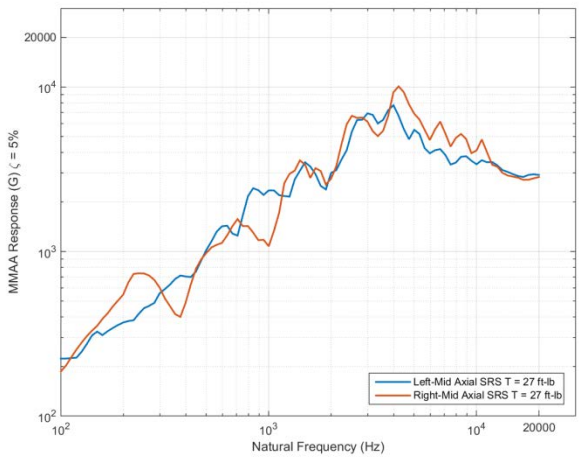

(b) SRS of Left-Mid and Right-Mid Node Set Average Axial Accelerations (T = 27 ft-lb)

Figure 19. SRS Before and After the Lap Joint

B. Experimental Results

The Brake-Reuss beam was suspended in a free-free configuration and axial impacts, shown in Figure 20, were applied at the right end. The impact amplitudes were ~100X smaller than those in the simulations. The beam was tested with two levels of bolt torque (Table 2), and a solid beam was used as a reference to verify the data-processing MATLAB scripts. The solid beam was monolithic, so its modal properties differ from the bolted lap joint beam; it would have been preferable to use a solid beam with the holes and bolts, but it was not available. Accelerometers were placed on both sides of the joint, about 11" from each end, and about 4.75" from the end where the force was applied as illustrated in Figure 21.

Table 2. Brake-Reuss Beam Test Configurations

Beam Type	Bolt Torque	Fundamental Axial Free-Free Frequency (Hz)	Impact Force Range (N)
Monolithic	N/A	3453	90 - 392
3 Bolts	11 ft-lb	2778	90 - 440
3 Bolts	27 ft-lb	2787	106 - 477

Although the excitation was not characteristic of pyroshock, and the impact forces were small, the experimental data provide some insight into attenuation characteristics. First, the amount of bolt preload did not have an appreciable effect on the attenuation across the joint. The low level of the applied force was likely the dominant reason that no difference was observed; the joint likely did not experience micro-slip or macro-slip from the impact. However, the SRS attenuation magnitude varied from -12 dB to +6 dB (Figure 22) depending on the natural frequency. The SRS suggest that the attenuation effects may be within the uncertainty due to measurement location. This effect also was observed in the spacecraft case study described in Section B.

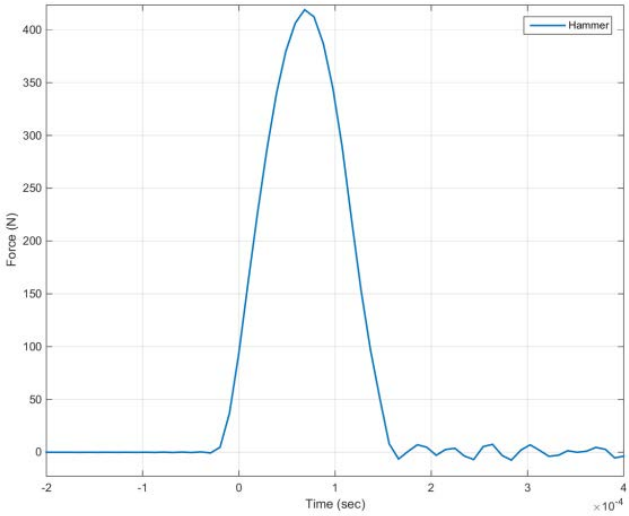

Figure 20. Hammer Impact Force

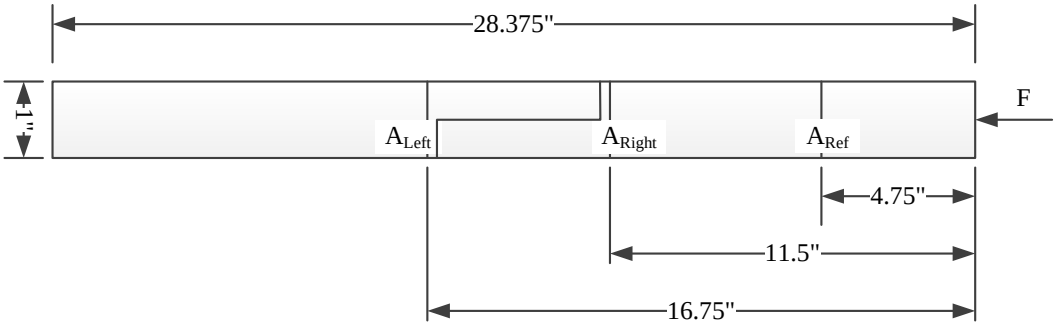

Figure 21. Beam Sensor and Loading Locations

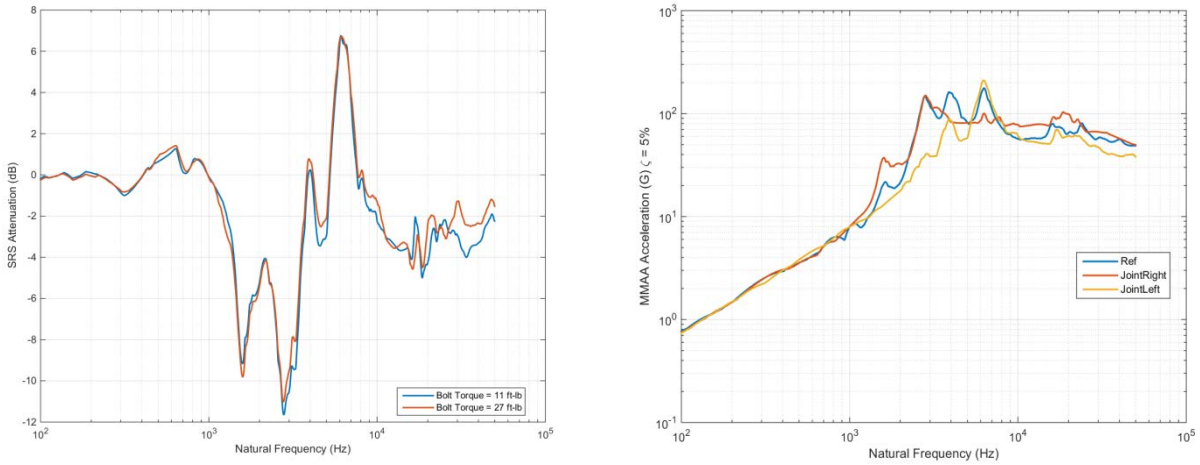

(a) SRS Attenuation across the Joint (b) Measured SRS (Bolt Torque = 11 ft-lb)

Figure 22. Attenuation in the Beam across the Lap Joint and Measured Shock Response Spectra

V. Conclusion

From a system's perspective, it is desirable to estimate attenuation factors for pyroshocks with conservative accuracy. If the attenuation factor is too low, the structural design will be negatively affected; on the other hand if high shock attenuation factors are used then shock sensitive parts may suffer damage during environmental testing or in-service. The greatest challenge in predicting shock attenuation in a complex structure is the amount of variability in the response to a pyroshock. Because pyroshocks have high frequency energy, the spatial and spectral sensitivity can be significant.

The shock attenuation data compiled in the 1960's – 1980's were for specific spacecraft and launch vehicles of the day. These data were included in NASA and MIL standards and handbooks. No uncertainty bounds were calculated and are not generally known or used explicitly although the variability can be rather large, therefore the attenuation models should be used with appropriate derating factors (i.e., factors of safety). These will be program specific and no recommendations are made herein.

A case study was presented that compared predicted shock attenuation with test measured shock attenuation levels. The predicted attenuation factors sought to take into account vehicle specific geometry and shock path characteristics. The data showed that the predicted levels of attenuation were unconservative at natural frequencies below the knee frequencies and generally conservative at natural frequencies above the knee frequency. However, there was a large amount of variability in the measured data depending on the placement of the sensor. This confirmed the sensitivity of shock attenuation to specific structural features that are often unknown early in a program when component level environments are first established.

High-performance finite element software has the potential to improve shock attenuation models. A numerical study of shock propagation through a lap joint in a beam was performed using Sandia National Laboratories Sierra Solid Mechanics finite element code. The simulations showed no attenuation in the axial direction through the lap joint. This study also showed that the modeling effort can be substantial and the computational run times quite long. Finite element modeling tools are not ready for detailed shock response predictions of (small) shock sensitive components. However, the tools may provide the capability to better understand the shock attenuation effects of joint categories and structural interfaces. These can replace experiments and inform shock attenuation predictions.

Acknowledgments

Sandia is a multi-program laboratory managed operated by Sandia Corporation, a wholly owned subsidiary of Lockheed Martin Company, for the U.S. Department of Energy's National Nuclear Security Administration under Contract DE-AC04-94AL85000.

References

[1] Himelblau, H., et al., *Dynamic Environmental Criteria*, NASA-HDBK-7005, March 13, 2001.

[2] --------, *Spacecraft Dynamic Environments Testing*, NASA-HDBK-7008, June 12, 2014.

[3] --------, *Pyroshock Test Criteria*, NASA-STD-7003A, December 20, 2011.

[4] --------, *General Environmental Verification Standard (GEVS) for GSFC Flight Programs and Projects*, GSFC-STD-7000A, April 22, 2013.

[5] Kacena, W.J, McGrath, M.B., and Rader, W.P., Aerospace Systems Pyrotechnic Shock Data (Ground Test and Flight), Vol. 1, Summary and Analysis, NASA-CR-116437, March 7, 1970.

[6] Kacena, W.J, McGrath, M.B., and Rader, W.P., Aerospace Systems Pyrotechnic Shock Data (Ground Test and Flight), Vol. 6, Pyrotechnic Shock Design Guidelines Manual, NASA-CR-116406, March 7, 1970.

[7] Barrett, S., "The Development of Pyro Shock Test Requirements for Viking Lander Capsule Components," *Proceedings of the Institute of Environmental Sciences 21st Annual Technical Meeting*, pp. 5-10, April 14-16, 1975.

[8] --------, *Environmental Engineering Considerations and Laboratory Tests*, MIL-STD-810G, October 31, 2008.

[9] --------, *Test Requirements for Launch, Upper-Stage and Space-Vehicles*, MIL-HDBK-340A, April 01, 1999.

[10] --------, *Test Requirements for Launch, Upper-Stage and Space-Vehicles*, Space and Missile Systems Center Standard SMC-016, September 05, 2014.

[11] White, J.D., Larsen, G.A., and Hanifen, D.W. (ed.) *Space Vehicle Test and Evaluation Handbook*, 2nd Edition, Aerospace Report No. TOR-2011(8591)-2, Vol. 1, 2012.

[12] Sarafin, T.P., *Spacecraft Structures and Mechanisms – From Concept to Launch*, Space Technology Series, 2007.

[13] Lalanne, C., *Mechanical Shock, Mechanical Vibration and Shock Analysis Series*, 3rd edition, Vol. 2, John Wiley & Sons, New Jersey, 2014.

[14] Brake, M.R, Reuss, P., Segalman, D.J., and Gaul, L., "Measurements and Modeling of Variability and Repeatability of Jointed Structures with Frictional Interfaces," *IMAC XXXII A Conference and Exposition on Structural Dynamics*, Orlando, FL, 2014.

[15] Kolaini, A. R., and Fernandez, J.P., "Qualifying Flight Hardware for Pyroshock Environments: Shock Simulation Systems and Modeling," *2nd Workshop on Spacecraft Shock Environment and Verification*, ESA/ESTEC, The Netherlands, 2015.
[16] Papadopoulos, L., "Shock Prediction Study and Lessons Learned from a Space Vehicle Shock Test," *Spacecraft and Launch Vehicle Dynamic Environments Workshop*, The Aerospace Corporation, 2016.